

KidneyRegNet: A Deep Learning Method for 3DCT-2DUS Kidney Registration during Breathing

Chi Yanling^{1*#}, Xu Yuyu^{2*}, Liu Huiying¹, Wu Xiaoxiang², Liu Zhiqiang², Mao Jiawei³, Xu Guibin^{2#}, Huang Weimin^{1#}

¹Institute for Infocomm Research, Agency for Science, Technology and Research, 1 Fusionopolis Way #21-01 Connexis South, Singapore 138632, {chiyl, liuhy, wmhuang}@i2r.a-star.edu.sg

²Key Laboratory of Biological Targeting Diagnosis, Therapy and Rehabilitation of Guangdong Higher Education Institutes, The Fifth Affiliated Hospital of Guangzhou Medical University, 510700, China, gyxyy@foxmail.com, 348215424@qq.com, {zhiqiang_liu2012, gyxgb}@163.com

³Creative Medtech Solutions Pte Ltd, mao.jiawei@ultrastmedtech.com

*Equal contribution authors, #Correspondence authors

ABSTRACT

This work proposed a novel deep registration pipeline for 3D CT and 2D U/S kidney scans of free breathing, which consists of a feature network, and a 3D-2D CNN-based registration network. The feature network has handcraft texture feature layers to reduce the semantic gap. The registration network is encoder-decoder structure with loss of feature-image-motion (FIM), which enables hierarchical regression at decoder layers and avoids multiple network concatenation. It was first pretrained with retrospective datasets cum training data generation strategy, then adapted to specific patient data under unsupervised one-cycle transfer learning in onsite application. The experiment was on 132 U/S sequences, 39 multiple phase CT and 210 public single phase CT images, and 25 pairs of CT and U/S sequences. It resulted in mean contour distance (MCD) of 0.94 mm between kidneys on CT and U/S images and MCD of 1.15 mm on CT and reference CT images. For datasets with small transformations, it resulted in MCD of 0.82 and 1.02 mm respectively. For large transformations, it resulted in MCD of 1.10 and 1.28 mm respectively. This work addressed difficulties in 3DCT-2DUS kidney registration during free breathing via novel network structures and training strategy.

Introduction

Medical image registration is a process that aligns one image to another originated from same or different modality. This aligned image contains more spatial-temporal information, which is important for applications such as image guided surgery, disease monitoring and risk prediction. Registration between images of same modality is mono-modal registration, and of different modality is multi-modal registration. Different imaging techniques are sensitive to different tissues in the body. Therefore, images of different modalities need to be registered to each other to provide complementary information. However, it is difficult because of the complex relationship between the intensities of corresponding structures in the two images. Ultrasound (U/S) images are especially challenging due to the large motion, small field of view and low scan quality. Nonetheless, 3D-2D registration is required. The potential of deep learning on those issues has not fully reached [1]. In this work, we proposed deep learning method to tackle 3D computed tomography (CT) to 2D ultrasound (3DCT-2DUS) kidney registration.

State-of-the-arts (SOTA) methods [2] can be classified as supervised, weakly supervised and unsupervised registration according to learning strategy, or convolutional neural network (CNN) based, deep adversarial network based, and transformer based image registration, according to baseline network architecture. The supervised registration [3] is trained to predict the transformation by using images and their ground truth transformations. Weakly supervised registration [4] [5] [6] uses overlapping segmentations of anatomical structures as loss function, which lowers the limitations associated with ground truth data. Unsupervised registration [7] [8] [9] [10] [11] [12] is trained by minimising a dissimilarity measure given a set of images and does not need ground truth transformations. CNN-base image registration [13] [14] trains a designed CNN architecture and learns the mapping between the input images and the deformation fields. Deep adversarial image registration [15] [16] consists of a generator network and a discriminator network. The generator network is trained to generate transformations and the discriminator network learns similarity metric to ensure the generated transformations being realistic, or the input images being well-registered. Vision Transformer (ViT) based registration [17] [18] [19] [20] [21] learns the data inherent relationships through the attention mechanism. Our solution is CNN-based unsupervised registration. We refer registration to unsupervised learning due to that the feature subnets are trained separately and not specifically for the registration task. The subnets are independent feature extractor, and universal features are also applicable to our solution.

Most of 3D-2D registration is supervised projective registration. The 2D image is the projection of the 3D volume. Miao [3] proposed to use CNN regression to register 2D X-ray images with 3D Digitally Reconstructed Radiograph (DRR) images. Ground truth transformations were available for their application. Foote [22] proposed to track tumour using a single fluoroscopic projection via supervised learning based method. The method densely sampled the CT volumes and calculated DRR projections with a linear combination of motion components via DenseNet [23]. Liao [24] and Krebs [25] [26] proposed to employ reinforcement learning to conduct 2D/3D registration by learning a serial of actions. Ours is sliced 3D-2D registration. No assumption of projective geometry is made and no ground truth is available. Besides, it faces challenges of very large potential searching space. We handle those difficulties using the proposed novel solution. Wei [27] proposed to register vessel labels on 2D U/S image to vessel labels on 3DCT/MR liver images using deep registration, which was mono-modal approach. They labelled the image manually and did not analyse the complex relationship between the intensities of corresponding structures in multimodality images. They tested the method on synthetic or phantom data, and the performance on clinical datasets was unknown.

Deep affine registration uses encoder structure [11], Siamese encoder structure [39] or ViT based structure [38]. They are 3D-3D single modality image registration and cannot be the full solution for 3DCT-2DUS registration. Moreover, for registration in multiple scales, two or three encoders are stacked together due to capacity limitation. Different from them, we proposed to use encoder-decoder structure, which enable multiple scale registration by hierarchical regression of transformation parameters from decoder layers. It allows more scales and benefits large transformation registration and fast model converge.

Balakrishnan [7] proposed VoxelMorph to do unsupervised registration. We adopted their baseline architecture and improved to a hierarchical architecture to generate transformation parameters in multiple scales. Hu [5] proposed to use image features to guide the registration. Our work is superior to their work [5] conceptually in several aspects. The first one is on architecture. In their work, original images are used to train registration network and the ground truth image segmentation labels are used to calculate loss function. Our work uses a network to represent images and inputs image representations to registration network. Both of voxel level image content and high-level features contribute to registration. The second one is loss function. A modality independent neighbourhood descriptor (MIND) [28] is used to measure image similarity of CT-US pair. Here, we assume high-level feature can drive alignment close to its optimal and MIND loss is continuous locally. A gradient loss is designed to regularize respiration motion smoothness on windowed U/S scans. The third is they tackle 3DCT-3DTRUS prostate registration. We tackle 3DCT- 2DUS kidney using a deep rigid registration. We pre-train a model by using unsupervised learning cum data generation scheme, and refine the model by one-cycle transfer learning. Heinrich [29] proposed a discrete 3DCT-CT registration, which used two steps of optimizations, unsupervised learning for global searching and correlation layer for local optimal search. Ours integrates feature, image, and motion metric into the loss function and conducts one-step transformation estimation.

In this work, we contributed a novel deep learning pipeline for sliced 3DCT-2DUS kidney registration. It overcame two main challenges: to register images of different dimensions and imaging modalities. To tackle the dimension difference, the U/S images were first expanded to the same dimension of CT by zero padding. Because there were relatively few spatial constrains between CT volume and 2D U/S slices compared with 3D-3D volume registration, it required to move 3D CT effectively. We proposed using a rigid encoder-decoder registration network and hierarchical regression of transformations from each decoder level. Transformations for images from low to high resolutions were combined at highest resolution via weighted translation and rotation. Besides hierarchical regression, we designed a combined loss to drive image sequence alignment accurately via global deep kidney feature and local modality independent image feature, and smoothly via transformation of consecutive frames. Moreover, to further improve the registration performance and be efficient in clinical application, we proposed to unsupervised train the registration network in two steps: pre-train the model using the general training datasets, and adaptively train the model two epochs using specific patient training datasets by one cycle transfer learning. A training data generation was proposed to generate image pairs for general training. To tackle the different imaging modalities, we proposed to extract deep kidney features on CT and U/S images for overall comparison and extract modality independent image features for comparison with local details. The feature network was designed with handcraft texture layers to reduce the semantic gap. Furthermore, we applied a time window on U/S sequence to improve kidney observation on noisy images by including respiration motion information. Generally, the methodology addressed all issues in kidney registration during free breathing. To the best of our knowledge, it is the first deep learning pipeline for sliced 3DCT-2DUS kidney registration.

Methods

The human kidney seldom deforms due to patient posture changes and respiration according to clinicians. Therefore, we use rigid transform in the kidney image registration. The proposed solution consists of 3DULBNet [30] and a 3D-2D

hierarchical registration network. 3DULBNet is trained on CT and windowed U/S images on binary segmentation tasks separately offline. They are connected with registration network to predict the CT plane that best aligned with U/S images.

Feature Network

The ULBNet (Fig.1) is a 5-level U-Net with residual block replacing the original convolutional layer. A local binary convolution (LBC) layer [31] is added to skip connections. The dropout rate is set 0.2. For CT images, the patch size is $160 \times 160 \times 80$ and batch size is 1. The optimizer is Adam. The loss function is minus dice coefficient. The output layer is a convolutional layer with sigmoid activation, and its output is kidney feature map of CT images. One can refer [30] for details on CT images.

U/S image is noisy and it is difficult to delineate kidney from a single image. The kidney motion information is useful. Since the U/S sequence scans kidney in respiration, the kidney motion can not be observed in one frame but can be observed in a few consecutive frames. The U/S image sequences are experimentally windowed with size of 5. Thus, instead of extract feature from 2D U/S frame, we extract it from volume in $256 \times 192 \times 5$. In U/S feature net, the input size is $256 \times 192 \times 5$ and down/up sampled by 2 at each levels. We do not down sample the data in the time dimension. The number of feature maps are 16, 32, 64, 128, 256 in encoder pathway, and 256, 128, 64, 32, 16 in decoder pathway. The output layer is a convolutional layer with sigmoid activation and outputs U/S kidney feature map. Kidney feature maps of CT and U/S images are of same dimension as input. The windowed kidney feature images construct CT-US image pair.

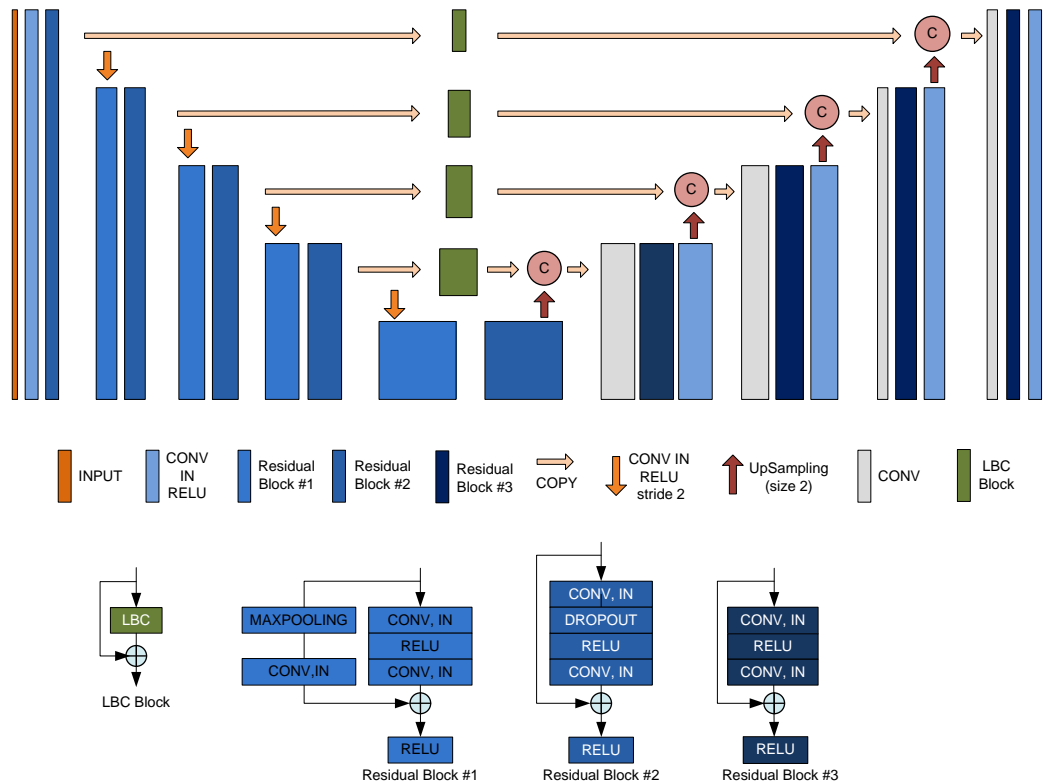


Figure 1. The 3D ULBNet network architecture.

Registration Network

We presented kidney registration (Fig. 2) in five aspects: image pair pre-processing, network structure, loss function, training data generation and learning strategy.

Pre-processing

All CT images are converted to RAI orientation and isotopically sampled in $0.8\text{mm} \times 0.8\text{mm} \times 0.8\text{mm}$. CT scans are automatically cropped to $128 \times 224 \times 288$ around centroid. An U/S image is resampled to $0.8\text{mm} \times 0.8\text{mm}$ and cropped to 224×288 . Windowed U/S images are centred in a $128 \times 224 \times 288$ volume with zero padding. Within one U/S window, the middle is the registration target and the others contribute to motion regularization. U/S images are stacked along the time axis, same as R-L axis in image space. CT volume is aligned with U/S by matching the kidney centroids from feature maps. Because U/S scanning of kidney is subject to the constraints of rib and spines of patients, the variability of the

initial position of 3DCT-2DUS pairs can be in large. To reduce variability, we uniformly align the kidney on CT in inferior-superior axis and then align with kidney on U/S with centroid. The inputs to the registration network are CT and U/S window image of $128 \times 224 \times 288$. CT is the moving image and U/S is the fix image.

Network Structure

The architecture is shown in Figure 2. CT and U/S volume are concatenated before going to the convolution layer. The number of feature maps are 8, 16, 16 in encoder pathway, and 16, 16, 16, 16, 8, 8 in decoder pathway. Up sampling is done using Upsampling3D and down sampling is done with stride convolution. Transformation regression uses the affine block. At each decoder level, activation of output (dense) layer is tanh for transformation parameters. The spatial transformer network (STN) layer [32] processes rigid transformation because kidney seldom has deformation during free respiration. Optimizer is Adam. The learning rate is $3e-4$. Given the window size of U/S images is N_w , the output transformation is a set of $6N_w$ rigid transformation parameters, $3N_w$ for rotation and $3N_w$ for translation. N_w is experimentally set 5 in this work. Each layer in decoder pathway outputs a set of transformation parameters, their weighted sum composes the final transformation. For rotation, it is an average of rotation parameters. For translation, it is a weighted sum of the translation parameters, the weights are $\{8, 4, 2, 1\}/4 = \{2, 1, 0.5, 0.25\}$. Rotation is scale invariance and is averagely weighted. Translation is inversely proportional to the image resolution and is proportionally weighted. The hierarchical activation improves prediction and shortens the training time. The number of trainable parameters is about 282M.

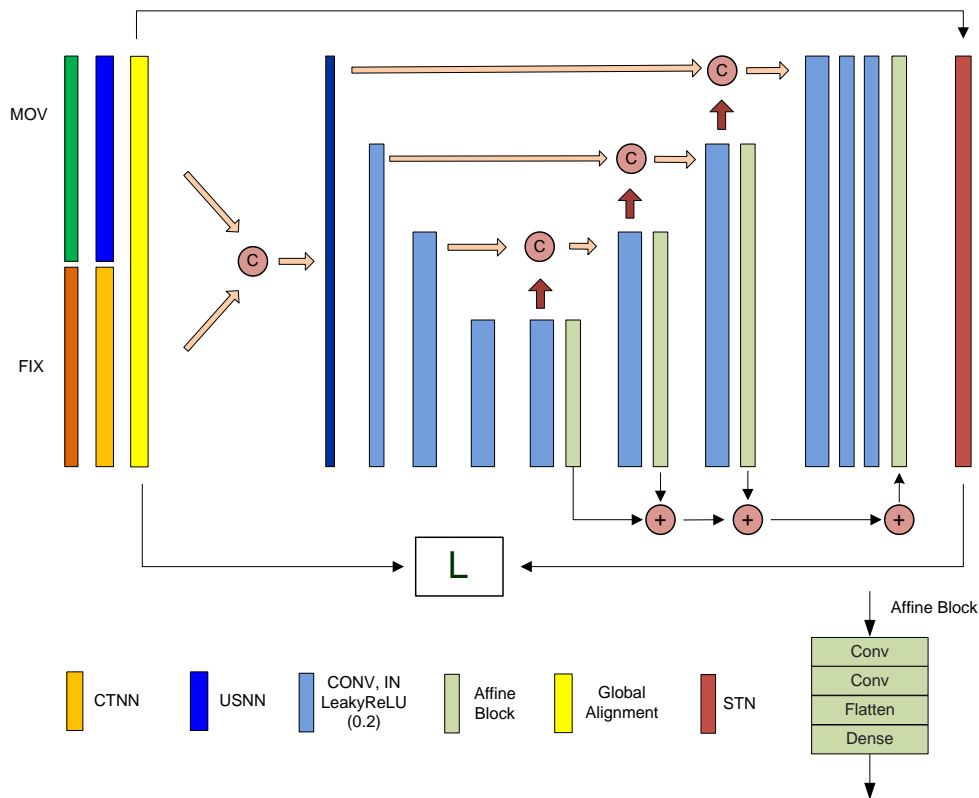


Figure 2. The 3D-2D registration network structure.

Loss function

The feature map describes overall kidney and MIND feature describes image details. They can complement with each other to measure alignment accurately. As registration is during breathing, CT cutting planes obtained should be able to stack together as smooth time sequences. Given I_{fix} fix image, I_{mov} moving image, M_{fix} fix feature map, M_{mov} moving feature map, \mathcal{D} transformation parameters, Feature-Image-Motion (FIM) loss is defined (Equ(2)) by three measure on feature map, original image, and transformation,

$$\begin{aligned} \mathcal{L}(I_{fix}, I_{mov}, M_{fix}, M_{mov}, \mathcal{D}) \\ = \mathcal{L}_f(M_{fix}, \mathcal{D} \circ M_{mov}) + \lambda_1 \mathcal{L}_i(I_{fix}, \mathcal{D} \circ (I_{mov} \cdot M_{mov})) + \lambda_2 \mathcal{L}_d(\mathcal{D}) \end{aligned} \quad (2)$$

$$\mathcal{L}_f(M_{fix}, \mathcal{D} \circ M_{mov}) = -\frac{1}{N_w} \sum_{i \in N_w} DICE_i(M_{fix}, \mathcal{D}_i \circ M_{mov}) \quad (3)$$

$$\mathcal{L}_i(I_{fix}, \mathcal{D} \circ (I_{mov} \cdot M_{mov})) = \frac{1}{|N|} \sum |MIND(I_{fix}) - MIND(\mathcal{D} \circ (I_{mov} \cdot M_{mov}))| \quad (4)$$

$$\mathcal{L}_d(\mathcal{D}) = 0.01 * \frac{\|\mathcal{D} - I_{4 \times 4}\|}{N_w} + 0.99 * grad\mathcal{D} \quad (5)$$

$$grad\mathcal{D} = \frac{1}{N_w - 2} \sum_{i-1, i, i+1 \in N_w} \|D_{i+1} + D_{i-1} - 2D_i\|$$

The feature loss is the minus dice coefficient of fix and warped kidney feature map (Equ (3)), where $DICE(x, y) = \frac{1}{m} \sum \left(\frac{2x \odot y}{x \oplus y} \right)$, \odot and \oplus are element-wise operations: multiplication and addition, m is number of elements. The image loss is the MIND between fix and warped original image (Equ (4)) [33]. A MIND feature is calculated by a Gaussian function of the mean squared difference between a central patch of the image and one of its six neighbouring patches. MIND loss is the mean absolute differences between the MIND features of CT and U/S images to compare two images with local details. N is the set of displacement vectors. Here, it needs to mask the CT images before calculating MIND because CT images display extra anatomic structures besides kidney. The transformation loss (Equ (5)) is a weighted sum of the L2-norm divided by the number of parameters, and the average transformation difference (Equ(6)). λ_1, λ_2 are set as 0.01 and 0.001 empirically. Here, we assume MIND is locally continuous. λ_1 is set 0.01 to make sure that feature loss dominates weight updates initially, and with approaching to the global optimal, image loss takes effect to fine tune the weights. The transformation loss is to regularize the motion transformation to move CT to its optimal position aligned with U/S images. Basically, feature loss, \mathcal{L}_f , is calculated on kidney feature maps. Image loss, \mathcal{L}_i , is computed between U/S images and masked CT images. Loss is calculated on kidney regions, thus, eliminates influence from difference between field of views in CT and U/S images.

Training Data Generation

The transformation is in 6-dimensional space, while the data size is relatively small. Network training prone to overfitting. Training dataset generation is necessary and has been employed in projective 3D-2D image registration [22] [34]. Densely sampling is commonly used. Unlike projective registration, the transformation parameters or its distribution for sliced 3D-2D registration is uncontrollable and unavailable. We need to find it out. First, we verified reference planes with clinicians. The transformations to obtain those verified alignments are modelled, parameter-by-parameter, in 2-sigma Gaussian distributions, where we randomly sampled N_t transformations individually. The N_t inverse transformations transform the optimal alignment back to N_t different initial kidney position. We generated N_t times training CT-US pairs by applying N_t inverse transformations on a reference CT volume. Our training data generation scheme helps to obtain much realistic training datasets to overcome overfitting. In the future, if sufficient clinical data is available, data generation can be neglected.

Learning Strategy

Based on the generated training datasets, unsupervised learning is employed to pretrain a registration model. In view that our target U/S images are respiration sequences including images of periodic breathing cycles. It is possible to make use the onsite patient specific dataset to improve the model performance further. We proposed one-cycle transfer learning strategy, which refine the pre-trained model using the first respiration cycle data via transfer learning with two epochs and infer the transformations sub-sequentially. We needs a pretrained model, because training from scratch is time consuming to converge with only one cycle train dataset available. It is impractical when long operation preparation time is disallowed. We propose using transfer learning to refine the model to save time and improve performance.

Experimental Data

Clinical Datasets

The datasets consists of public KiTS19 [35] datasets and in-house datasets. Public datasets consist of 210 corticomedullary phase (CMP) CT images. The in-house datasets were collecting from the fifth affiliated hospital Guangzhou Medical University, approved by the Institutional Review Board on Aug 28, 2020 with protocol number of L2020-24. The datasets were consecutively studied from January to May 2021, consisting of 132 U/S image sequences (more than 30K images) from 31 patients, 39 multiple phase CT images from 24 patients, and 25 pairs of CT volumes and U/S sequences from 25 patients. All images were anonymized. The CT scans were acquired on one 64-slice scanner (GE OPTIMA CT600 CT

scanner), using a standard four-phase contrast-enhanced imaging protocol with the slice thickness of 0.6–5.0mm, matrix of 512×512 pixels and inplane resolution of 0.625–0.916mm. CMP scanning was performed with 180 HU detected at region of interest within abdominal aorta. Nephrographic Phase (NP) phase was performed 28s post contrast, and excretory phase (EP) was performed 10–30 min post contrast. The U/S datasets were acquired on GE Versana Active™ ultrasound system, with matrix of 1132×852 pixels and in-plane resolution of 0.22–0.29 mm. The U/S sequences were scanned at 17-22 frames per second, and had 58±14 U/S images per respiration cycle.

Generated Training Datasets

Reference planes: For each U/S frame, a manually selected reference CT cutting plane with the overlap of kidney boundaries were displayed side-by-side to four experienced clinicians to unanimously verify if they were same cutting plane of the kidney. The verified planes constructed our basic reference set, from which we extended the training set. There are 22 out of 25 pairs of CT volume and U/S sequences verified by clinicians that their 3D cutting plane in CTs same as U/S images had been found.

Transformation Parameter Estimation: Six parameters in transformations that resulted in the reference CT planes from initial positions were modelled in 2-sigma Gaussian distributions. The clinical datasets were split in a ratio of 7:1:2 for training, validation and testing set according to patients. Only training datasets were generated by N times. They were normalized to pixel having zero mean value and one variance value. The 5-fold cross validation was used to evaluate the model’s performance.

Evaluation Metrics: Hausdorff distance (HD) and mean contour distance (MCD) between the outlines of kidney on CT and U/S images were used to evaluate if CT-US pair was well aligned, and calculated as

$$D_{Hausdorff}(U, C) = \max \left\{ \max_{c \in C} \left\{ \min_{u \in U} \{d(c, u)\} \right\}, \max_{u \in U} \left\{ \min_{c \in C} \{d(u, c)\} \right\} \right\}, D_{mean} = \frac{\text{mean} \{d(u, c)\}}{|U \cap C|}$$

$d(u, c)$ was absolute value on distance map, c and u were contour points on CT and U/S images. HD and MCD were in millimetre. The CT to U/S (CT-US) distance was calculated between kidney boundaries on CT and U/S image. The CT to CT (CT-CT) distance between kidney contours on resulted CT plane and reference CT plane.

Experiments and Results

Evaluation on Feature Network

Our network was implemented on the tensorflow and training was done on workstation with dual Nvidia Quadro RTX 5000 of 16GB, and CPU memory of 256GB. The learning rate was 1×10^{-4} . The model is evaluated by

$$DICE = \frac{2|Y \cap \hat{Y}|}{|Y| + |\hat{Y}|}, \text{ Sensitivity} = \frac{|Y \cap \hat{Y}|}{|\hat{Y}|}, \text{ Specificity} = \frac{|Y \cap \hat{Y}|}{|Y|}$$

where \hat{Y} was prediction and Y was ground truth.

The model resulted in an average Dice coefficient of 96.88% on kidney segmentation in the plain phase CT images (Table 1). The network resulted in an average Dice coefficient of 96.39% on U/S images.

	DICE	Sensitivity	Specificity
CT	0.9688	0.9711	0.9667
U/S	0.9639	0.9736	0.9560

Table 1: Feature network performance on kidney segmentation in CT and U/S images.

Evaluation on Registration Network

The generated datasets were only used for training. The more datasets generated, the smaller MCD achieved. Here, we generated about 12000 training data pairs, 10 times of clinic datasets, to pre-train the registration network. We conducted ablation study on the method (Table 2). All the network components contributed on performance improvement. The hierarchical transformation regression at decoder layers contributed more than the MIND loss. One cycle transfer learning contributed the most.

Methods	Metric (mm)	CT-CT	CT-US
Ours	HD	3.97±1.37	3.80±0.87
	MCD	1.15±0.57	0.94±0.18
Without MIND Loss	HD	4.43±1.40	3.74±0.90
	MCD	1.38±0.56	0.98±0.23
Without Decoder Layers	HD	7.66±2.95	4.14±1.15
	MCD	2.45±1.10	1.02±0.20
Without Hierarchical Transformation regression	HD	8.15±3.94	4.16±0.97
	MCD	2.71±1.48	1.05±0.21
Without One Cycle Transfer Learning	HD	11.59±1.57	6.71±1.06
	MCD	4.09±0.65	2.03±0.29

Table 2: CT-US kidney registration performance in the ablation study with individual component removed.

Result Comparison

As our pipeline is the first for 3DCT-2DUS kidney registration, we can only compare our method with SOTAs [11], [36], [37] in terms of registration module (Table 3). We replaced our encoder-decoder hierarchical registration subnet with the encoder structures or transformer based registration module. That is, the input to SOTA is CT-US feature pairs after global alignment. VoxelMorph, ConvNet-affine [11], VTN-affine [36], and C2FViT [37] were trained on the general training datasets to converge. VoxelMorph uses affine block same as in our registration network to get rigid transformation parameters. ConvNet-affine, and VTN-affine have been implemented based on their papers while rigid transformation was employed.

Ours, with two-step training, was superior to all SOTAs when measured by HD and MCD (Table 3). The 2D CT-US distances were smaller than 3D CT-CT, because the distance in one dimension was overlooked. With one-step training strategy, our pre-trained model performed better than VoxelMorph with smaller 3D CT-CT distance, while larger 2D CT-US distance. It indicated hierarchical structures prevented from converging to a local optimal. Besides, it was found that our pre-trained model with hierarchical structures was covered at about 20-50 epochs during training, much faster than VoxelMorph, converge at about 200-300 epochs. In addition, transformer based method, C2FViT, performed better than CNN-based methods with one-step training strategy.

	Metric (mm)	One-step learning		Two-step learning	
		CT-CT	CT-US	CT-CT	CT-US
Ours	HD	11.59±1.57	6.71±1.06	3.97±1.37	3.80±0.87
	MCD	4.09±0.65	2.03±0.29	1.15±0.57	0.94±0.18
VoxelMorph	HD	12.21±1.87	5.99±0.93	8.15±3.94	4.16±0.97
	MCD	4.38±0.72	1.82±0.28	2.71±1.48	1.05±0.21
C2FViT	HD	10.36±1.77	6.42±0.84	9.93±1.72	5.64±0.90
	MCD	3.74±0.91	1.93±0.50	3.48±0.78	1.45±0.42
VTN-Affine	HD	12.18±1.86	5.58±1.01	7.66±2.95	4.14±1.15
	MCD	4.21±0.71	1.45±0.35	2.45±1.10	1.02±0.20
ConvNet-Affine	HD	11.58±2.43	6.72±1.34	4.56±1.55	3.89±0.91
	MCD	4.36±1.11	2.07±0.51	1.46±0.62	1.00±0.23

Table 3: Registration performance comparison with SOTAs using one-step learning strategy (without one cycle transfer training applied) and using two-step learning strategy (with one cycle transfer learning applied).

We compared our method with SOTAs using two-step training strategy, say all with one cycle transfer learning strategy applied (Table 3). Ours learned most from the transfer learning to improve the performance. ConvNet, a Siamese encoder structure, was second only to ours. C2FViT learned least. CNN-based method performed better than transformer based method with one cycle transfer learning for two epochs. Ours performed the best.

We averagely divided the CT-US image pairs into two groups sorted by transformations. Group A comprised datasets of small transformations, rotations of 10.37 ± 2.24 degrees and translation of 3.69 ± 0.95 mm. Group B comprised datasets of large transformations, rotations of 24.72 ± 2.28 degrees and translation of 5.04 ± 1.20 mm. Rotation and translation were separately calculated as L2-norm of components in x, y, z directions. All deep learning based method used two-step learning strategy. The performance on two groups was measured (Table 4). Our method performed best on both Group A and B. It was robust to large transformations.

methods	Metric (mm)	Group A		Group B	
		CT-CT	CT-US	CT-CT	CT-US
Ours	HD	3.58±1.37	3.85±0.32	4.36±1.46	3.75±0.83
	MCD	1.02±0.59	0.82±0.04	1.28±0.53	1.10±0.20
Voxel-Morph	HD	7.97±0.31	4.20±0.34	8.34±6.75	4.12±0.94
	MCD	2.63±0.02	0.95±0.04	2.79±2.49	1.15±0.23
C2FViT	HD	8.01±0.09	5.82±0.88	11.85±1.79	5.47±0.09
	MCD	3.38±0.65	1.37±0.23	3.57±0.58	1.53±0.10
VTN-Affine	HD	5.84±0.41	4.41±0.47	9.48±5.21	3.86±1.09
	MCD	1.83±0.13	0.95±0.02	3.08±1.94	1.09±0.20
ConvNet-Affine	HD	4.32±1.06	3.72±0.01	4.80±1.66	4.06±1.04
	MCD	1.28±0.43	0.83±0.04	1.64±0.72	1.16±0.28

Table 4: Registration performance on datasets with small and large transformations.

Example testing sequences of CT and U/S images were display in RAI orientation (Fig. 3). U/S frames and result CT planes in sagittal view were stacked along R-L orientation. The axial and coronal views provided dynamic information and R-L axis can represent time. Coronal view displayed the up and down kidney’s motion during respiration and axial view displayed back and forth kidney motion.

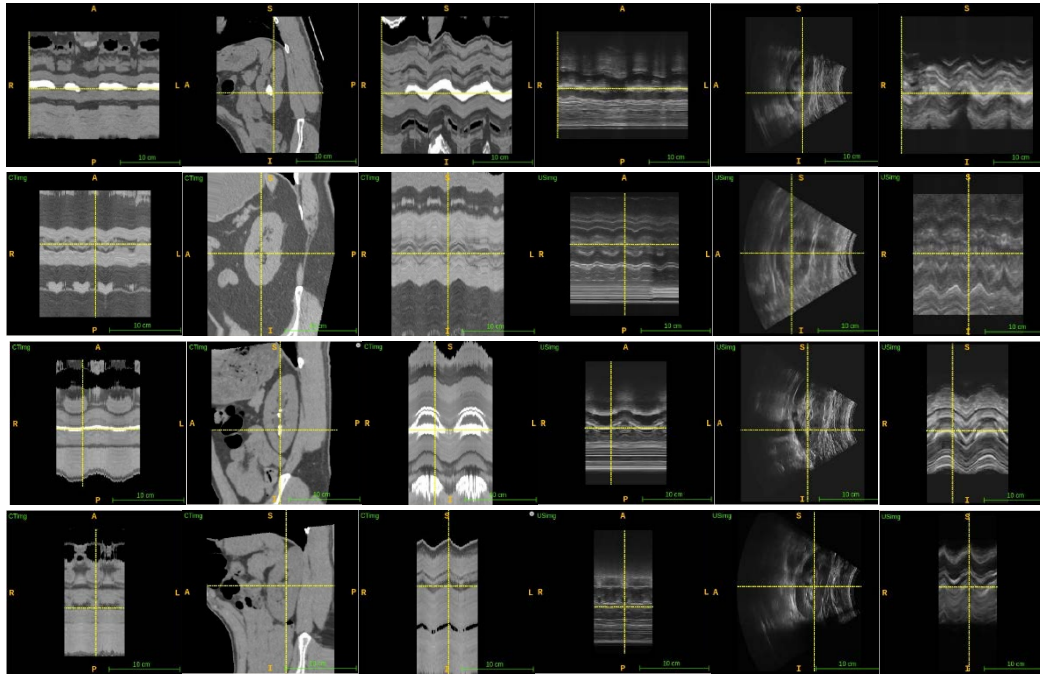


Figure 3. Example results, from left to right, the images are CT Axial view, CT Sagittal view, CT Coronal View, U/S Axial view, U/S Sagittal view, U/S Coronal View.

Finding corresponding landmarks between CT and U/S was difficult. We identified a special case, which had a small lesion visible on both the U/S images and CT images during breathing (Fig. 4). The lesion was about 7mm in diameter on the left kidney. It was interesting to know tumour distance after registration for this special case. If we assumed that the centre of the lesion observed on U/S scan was also its centroid on CT volume, a tumour center distance was 3.39 mm after registration. 4.38mm, 6.04mm, 4.16 mm, and 3.91 mm were resulted from VoxelMorph, C2FViT, VTN-affine, ConvNet-affine. The distance was big because the tumour was near the kidney surface.

Discussion

It is challenging to obtain perfect spatial correspondence for CT and U/S images. We measured the distance on the reference CT-US pairs, the average HD was $3.57±1.11$ mm, and MCD was $0.79±0.22$ mm that was around one pixel size. The distance is nonzero may be due to imperfect contour extraction, rib occlusion, or different patient postures.

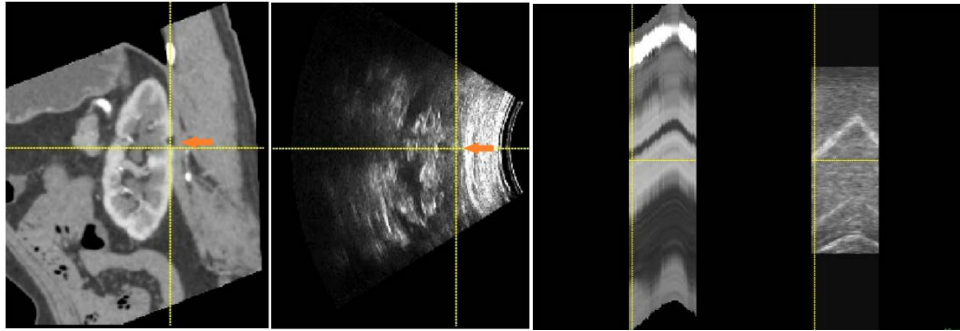


Figure 4. Example image pair to test on RTE (a) small lesion in CT image and U/S image, (b) small lesion motion in respiration.

The pre-trained model is benefited using training data generation, because the transformation parameters are in high dimensional space while data size is small. However, only increasing the generated datasets is difficult to improve the model performance further. We proposed to use transfer learning to achieve it.

Transfer learning may need extra preparation/training time before application. With pre-trained model, the preparation can be shortened significantly. For example, if registration model is trained from scratch using one-cycle learning, it takes about 46 mins to converge, while only 2-3 mins are needed if the model is trained using transfer learning. Thus, a good pre-trained model is essential to practical applications.

Even though optimal alignments verified with clinicians are available, we are not going to change our unsupervised learning to the supervised one. First, the data size is quite small and lots of efforts required to obtain more. It is not desirable to limit our model from processing versatile pairing data when available. The increased training data generates a regularization effect, which benefits the cost function optimization, reduction of overfitting, and model generalization. We believe, in the future, it is possible to collect more paired datasets to overcome overfitting resulted from the dataset's limitation.

Conclusions

This paper presented, to the best of our knowledge, the first deep learning pipeline for sliced 3DCT-2DUS kidney registration. All difficulties in kidney registration during free breathing have been addressed via novel network structures and training strategy. Comprehensive experiments showed that our proposed methodology performed well.

References

1. Nazib A, Fookes C, Perrin D (2018) A comparative analysis of registration tools: Traditional vs deep learning approach on high resolution tissue cleared data. arXiv preprint arXiv:181008315
2. Haskins G, Kruger U, Yan P (2020) Deep learning in medical image registration: a survey. *Machine Vision and Applications* 31:1–18
3. Miao S, Wang ZJ, Liao R (2016) A CNN regression approach for real-time 2D/3D registration. *IEEE transactions on medical imaging* 35:1352–1363
4. Heinrich MP (2019) Closing the gap between deep and conventional image registration using probabilistic dense displacement networks. In: *International Conference on Medical Image Computing and Computer-Assisted Intervention*. Springer, pp 50–58
5. Hu Y, Modat M, Gibson E, Li W, Ghavami N, Bonmati E, Wang G, Bandula S, Moore CM, Emberton M (2018) Weakly-supervised convolutional neural networks for multimodal image registration. *Medical image analysis* 49:1–13
6. Lee MC, Oktay O, Schuh A, Schaap M, Glocker B (2019) Image-and-spatial transformer networks for structure-guided image registration. In: *International Conference on Medical Image Computing and Computer-Assisted Intervention*. Springer, pp 337–345
7. Balakrishnan G, Zhao A, Sabuncu MR, Guttag J, Dalca AV (2019) Voxelmorph: a learning framework for deformable medical image registration. *IEEE transactions on medical imaging* 38:1788–1800

8. Dalca AV, Balakrishnan G, Guttag J, Sabuncu MR (2018) Unsupervised learning for fast probabilistic diffeomorphic registration. In: International Conference on Medical Image Computing and Computer-Assisted Intervention. Springer, pp 729–738
9. Kori A, Krishnamurthi G (2019) Zero shot learning for multi-modal real time image registration. arXiv preprint arXiv:190806213
10. Krebs J, Mansi T, Mailhé B, Ayache N, Delingette H (2018) Unsupervised probabilistic deformation modeling for robust diffeomorphic registration. In: Deep Learning in Medical Image Analysis and Multimodal Learning for Clinical Decision Support. Springer, pp 101–109
11. de Vos BD, Berendsen FF, Viergever MA, Sokooti H, Staring M, Išgum I (2019) A deep learning framework for unsupervised affine and deformable image registration. *Medical image analysis* 52:128–143
12. Yoo I, Hildebrand DG, Tobin WF, Lee W-CA, Jeong W-K (2017) ssemnet: Serial-section electron microscopy image registration using a spatial transformer network with learned features. In: Deep Learning in Medical Image Analysis and Multimodal Learning for Clinical Decision Support. Springer, pp 249–257
13. Cao X, Yang J, Zhang J, Nie D, Kim M, Wang Q, Shen D (2017) Deformable image registration based on similarity-steered CNN regression. In: International Conference on Medical Image Computing and Computer-Assisted Intervention. Springer, pp 300–308
14. Wu G, Kim M, Wang Q, Munsell BC, Shen D (2015) Scalable high-performance image registration framework by unsupervised deep feature representations learning. *IEEE Transactions on Biomedical Engineering* 63:1505–1516
15. Fan J, Cao X, Wang Q, Yap P-T, Shen D (2019) Adversarial learning for mono-or multi-modal registration. *Medical image analysis* 58:101545
16. Hu Y, Gibson E, Ghavami N, Bonmati E, Moore CM, Emberton M, Vercauteren T, Noble JA, Barratt DC (2018) Adversarial deformation regularization for training image registration neural networks. In: International Conference on Medical Image Computing and Computer-Assisted Intervention. Springer, pp 774–782
17. Baum Z, Hu Y, Barratt DC (2020) Multimodality biomedical image registration using free point transformer networks. In: *Medical Ultrasound, and Preterm, Perinatal and Paediatric Image Analysis*. Springer, pp 116–125
18. Chen J, Du Y, He Y, Segars WP, Li Y, Frey EC (2021) TransMorph: Transformer for unsupervised medical image registration. arXiv preprint arXiv:211110480
19. Chen J, He Y, Frey EC, Li Y, Du Y (2021) ViT-V-Net: Vision Transformer for Unsupervised Volumetric Medical Image Registration. arXiv preprint arXiv:210406468
20. Liu Z, Lin Y, Cao Y, Hu H, Wei Y, Zhang Z, Lin S, Guo B (2021) Swin transformer: Hierarchical vision transformer using shifted windows. In: *Proceedings of the IEEE/CVF International Conference on Computer Vision*. pp 10012–10022
21. Wang Z, Delingette H (2021) Attention for Image Registration (AiR): an unsupervised Transformer approach. arXiv preprint arXiv:210502282
22. Foote MD, Zimmerman BE, Sawant A, Joshi SC (2019) Real-time 2D-3D deformable registration with deep learning and application to lung radiotherapy targeting. In: International Conference on Information Processing in Medical Imaging. Springer, pp 265–276
23. Huang G, Liu Z, van der Maaten L, Weinberger KQ (2017) Densely Connected Convolutional Networks. pp 4700–4708
24. Liao R, Miao S, de Tournemire P, Grbic S, Kamen A, Mansi T, Comaniciu D (2017) An artificial agent for robust image registration. In: *Proceedings of the AAAI conference on artificial intelligence*
25. Krebs J, Delingette H, Mailhé B, Ayache N, Mansi T (2019) Learning a probabilistic model for diffeomorphic registration. *IEEE transactions on medical imaging* 38:2165–2176
26. Krebs J, Mansi T, Delingette H, Zhang L, Ghesu FC, Miao S, Maier AK, Ayache N, Liao R, Kamen A (2017) Robust non-rigid registration through agent-based action learning. In: International Conference on Medical Image Computing and Computer-Assisted Intervention. Springer, pp 344–352
27. Wei WEI, Haishan X, Alpers J, Rak M, Hansen C (2021) A deep learning approach for 2D ultrasound and 3D CT/MR image registration in liver tumor ablation. *Computer Methods and Programs in Biomedicine* 206:106117

28. Heinrich MP, Jenkinson M, Bhushan M, Matin T, Gleeson FV, Brady M, Schnabel JA (2012) MIND: Modality independent neighbourhood descriptor for multi-modal deformable registration. *Medical image analysis* 16:1423–1435
29. Heinrich MP, Hansen L (2020) Highly accurate and memory efficient unsupervised learning-based discrete CT registration using 2.5 D displacement search. In: *International Conference on Medical Image Computing and Computer-Assisted Intervention*. Springer, pp 190–200
30. Chi Y, Xu Y, Feng G, Mao J, Wu S, Xu G, Huang W (2021) Segmenting Kidney on Multiple Phase CT Images using ULBNet. In: *2020 25th International Conference on Pattern Recognition (ICPR)*. IEEE, pp 8554–8561
31. Pietikäinen M, Hadid A, Zhao G, Ahonen T (2011) *Computer vision using local binary patterns*. Springer Science & Business Media
32. Jaderberg M, Simonyan K, Zisserman A (2015) Spatial transformer networks. *Advances in neural information processing systems* 28:2017–2025
33. Heinrich MP, Jenkinson M, Papież BW, Brady SM, Schnabel JA (2013) Towards realtime multimodal fusion for image-guided interventions using self-similarities. In: *International conference on medical image computing and computer-assisted intervention*. Springer, pp 187–194
34. Schaffert R, Wang J, Fischer P, Borsdorf A, Maier A (2020) Learning an attention model for robust 2-D/3-D registration using point-to-plane correspondences. *IEEE transactions on medical imaging* 39:3159–3174
35. <https://kits19.grand-challenge.org/>
36. Zhao S, Lau T, Luo J, Eric I, Chang C, Xu Y (2019) Unsupervised 3D end-to-end medical image registration with volume tweening network. *IEEE journal of biomedical and health informatics* 24:1394–1404
37. Mok TC, Chung A (2022) Affine Medical Image Registration with Coarse-to-Fine Vision Transformer. In: *Proceedings of the IEEE/CVF Conference on Computer Vision and Pattern Recognition*. pp 20835–20844

Acknowledgement

This work is supported by ACCL/19-GAP035-R20H.

Competing Interests

The authors declare no competing interests.

Ethics Declarations

The in-house datasets were collecting from the fifth affiliated hospital Guangzhou Medical University, approved by the Institutional Review Board on Aug 28, 2020 with protocol number of L2020-24.

Appendix

Reference plane

For each U/S frame, a manually selected reference CT cutting plane with the overlap of kidney boundaries were displayed side-by-side to four experienced clinicians to unanimously verify if they were same cutting plane of the kidney. The verified planes constructed our basic reference set, from which we extended the training set. There are 22 out of 25 pairs of CT volume and U/S sequences verified by clinicians that their 3D cutting plane in CTs same as U/S images had been found (Fig. 1).

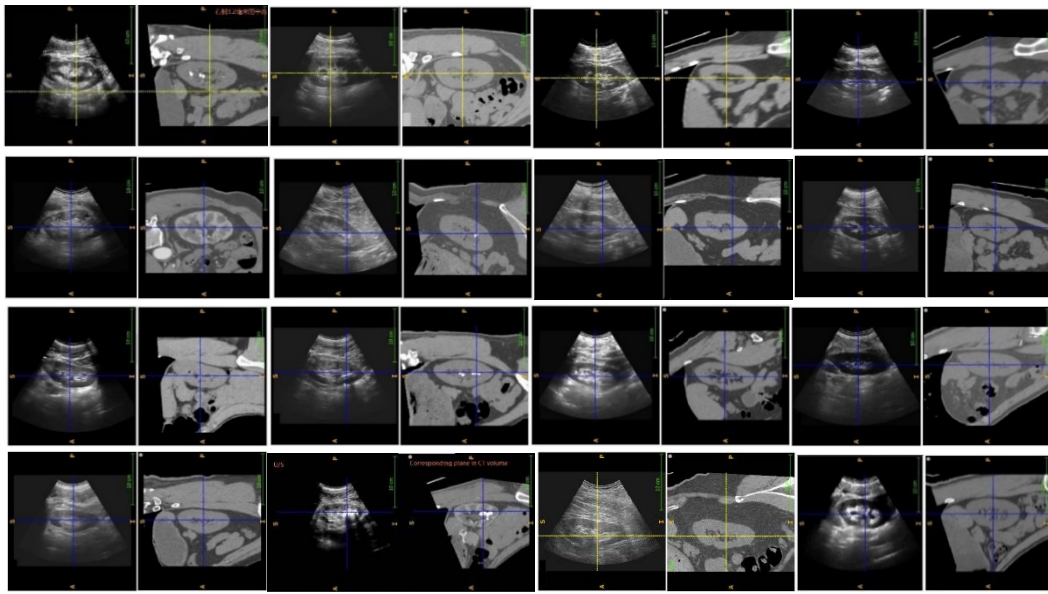


Figure 1. Examples of the verified reference planes.

Transformation Parameter Estimation

Six parameters in transformations that resulted in the reference CT planes from initial positions (Fig. 2), were modelled in 2-sigma Gaussian distributions.

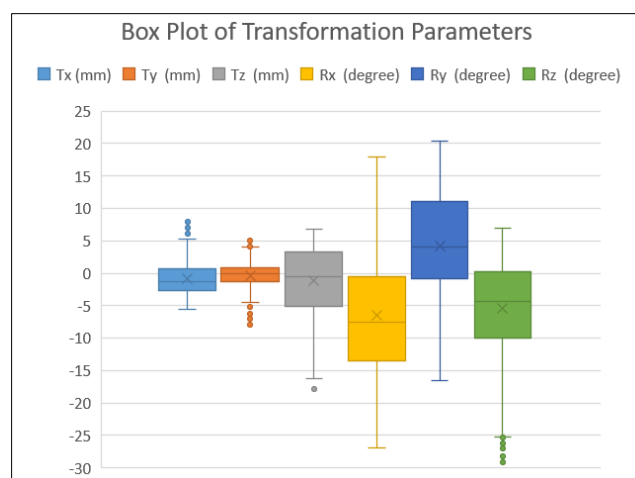


Figure 2. Distribution of transformation parameters (T: translation, R: Euler angle)

Generated Datasets

The generated datasets were only used for training. The more datasets generated, the smaller MCD achieved (Fig.3). A local minimum occurred at 6000 pairs. Global minimum occurred around 12000 pairs where the 3D CT-CT distance closed to 2D CT-US distance. Thus, we generated about 12000 training data pairs, 10 times of clinic datasets, to pre-train the registration network.

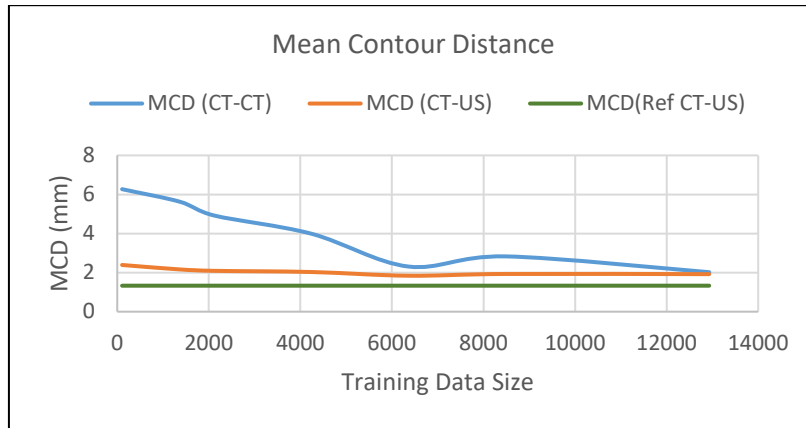


Figure 3. Average MCD decreases when generated training datasets increase.

U/S feature network performance on Window Size

We tested feature extraction on U/S image sequences with different window sizes (Table 1). The best performance obtained at size of 5.

Window size	DICE	Sensitivity	Specificity
1	0.9391	0.9492	0.9455
3	0.9543	0.9714	0.9407
5	0.9639	0.9736	0.9560
7	0.9604	0.9675	0.9561
9	0.9590	0.9656	0.9544

Table 1: Feature network performance on kidney segmentation in U/S images with different window size. The U/S images are of dimension $256 \times 192 \times \text{WindowSize}$.

Registration performance on transfer learning strategy

The model performance on four test sequences from second cycle was evaluated. Overall, one-cycle training performed best as observed in Table 2. Moreover, we found transfer learning helped to achieve a lower loss than model trained from scratch in Table3.

	Loss (Epoch = 2)		Loss _{min}	
	TFL	TFS	TFL	TFS
Case 01	-0.9744	-0.9681	-0.9773	-0.9762
Case 02	-0.9642	-0.9508	-0.9689	-0.9673
Case 03	-0.9624	-0.9507	-0.9706	-0.9699
Case 04	-0.9610	-0.9559	-0.9692	-0.9683
Average	-0.9655	-0.9563	-0.9715	-0.9704

TFL: training model via transfer learning, TFS: training model from scratch, Loss_{min}: the minimal loss obtained within 100 epochs.

Table 3: Feature-image-motion Loss obtained from two learning strategy: TFL and TFS.

	Metric (mm)		Learning strategy			
			Pre-trained model	One-shot (5epochs)	Five-shot (5epochs)	One-cycle (2epochs)
Case 01	CT-US	HD	7.25±1.22	3.99±0.86	3.20±0.72	3.01±0.73
		MCD	2.53±0.30	1.07±0.32	0.85±0.18	0.75±0.17
	CT-CT	HD	5.78±1.50	6.12±1.66	6.00±1.70	6.75±2.42
		MCD	2.03±0.56	2.06±0.56	1.80±0.52	2.17±0.95
Case 02	CT-US	HD	8.32±1.21	4.91±0.77	4.35±1.22	4.16±0.65
		MCD	2.11±0.46	1.61±0.70	0.95±0.20	0.85±0.13
	CT-CT	HD	19.18±2.66	4.52±1.34	4.80±1.69	4.45±2.09
		MCD	6.38±0.84	2.00±1.01	1.56±0.62	1.47±0.91
Case 03	CT-US	HD	5.39±0.72	4.89±0.90	3.61±0.99	3.54±1.11
		MCD	1.50±0.19	1.36±0.38	0.95±0.27	0.79±0.19
	CT-CT	HD	16.52±1.21	11.92±2.32	4.68±1.44	2.72±0.64
		MCD	5.70±0.39	3.93±0.82	1.64±0.84	0.58±0.26
Case 04	CT-US	HD	5.89±1.11	5.29±1.16	4.45±1.10	4.52±0.99
		MCD	1.99±0.23	1.75±0.28	1.43±0.23	1.40±0.23
	CT-CT	HD	4.90±0.92	4.68±0.85	2.94±0.79	1.98±0.34
		MCD	2.27±0.84	2.00±0.86	0.89±0.45	0.39±0.19
Average	CT-US	HD	6.71±1.06	4.77±0.92	3.90±1.00	3.80±0.87
		MCD	2.03±0.29	1.44±0.42	1.04±0.22	0.94±0.18
	CT-CT	HD	11.59±1.57	6.81±1.54	4.63±1.40	3.97±1.37
		MCD	4.09±0.65	2.49±0.81	1.47±0.60	1.15±0.57

The CT-US distance is calculated between kidneys boundaries on CT and U/S. The CT-CT distance between kidney contours on resulted CT plane and reference CT plane.

Table 2: 3DCT-2DUS Kidney registration performance on four learning strategies.

Registration Network Performance on Window Size

We tested registration on motion regularization with window size of 1, 3, 5 (Table 4), and size of 1 resulted in best accuracy, while size of 5 resulted in visually smoother CT cutting plane sequences. It was reasonable that the large window size gave a smooth regularization at the expense of accuracy. Size of 1 approached the global minimal by free transition and rotation, while size of 5 approached optimal transformation by transition in a larger scale due to the motion regularization. Since smoothness was also important, we selected 5 to achieve overall optimal.

WindowSize	Metric (mm)	CT-CT	CT-US
1	HD	2.91±1.11	3.73±0.95
	MCD	0.97±0.44	0.95±0.21
3	HD	3.39±1.38	3.82±0.96
	MCD	0.99±0.58	0.98±0.25
5	HD	3.97±1.37	3.80±0.87
	MCD	1.15±0.57	0.94±0.18

Table 4: CT-US registration performance on the number of consecutive frames (WindowSize) used for motion regularization.

Uncertainty Estimation

Due to the unavailability of ground truth for image registration, an uncertainty estimate would help gauge system reliability. Registration uncertainty was estimated by random taking out 1~10% training datasets and estimating the standard deviation of the performance. The experiment was repeated (n=10). The uncertainty in MCD was about 1mm for CT-CT distance and 0.22mm for CT-US distance (Table 5).

	CT-US		CT-CT	
	HD	MCD	HD	MCD
Standard deviation (mm)	1.62	0.22	2.97	1.01

Table 5: Performance variance of ten repeated experiments on CT-US registration with random training datasets taking out.

Registration Result Examples

We illustrated the registration results from two-step training strategy by plotting U/S image plane in CT volume (Fig. 4). The initial position (blue), the reference plane position (green), and the result plane position (red) can be observed in coronal view. Our method resulted in the closest cutting plane to the reference plane than the other methods.

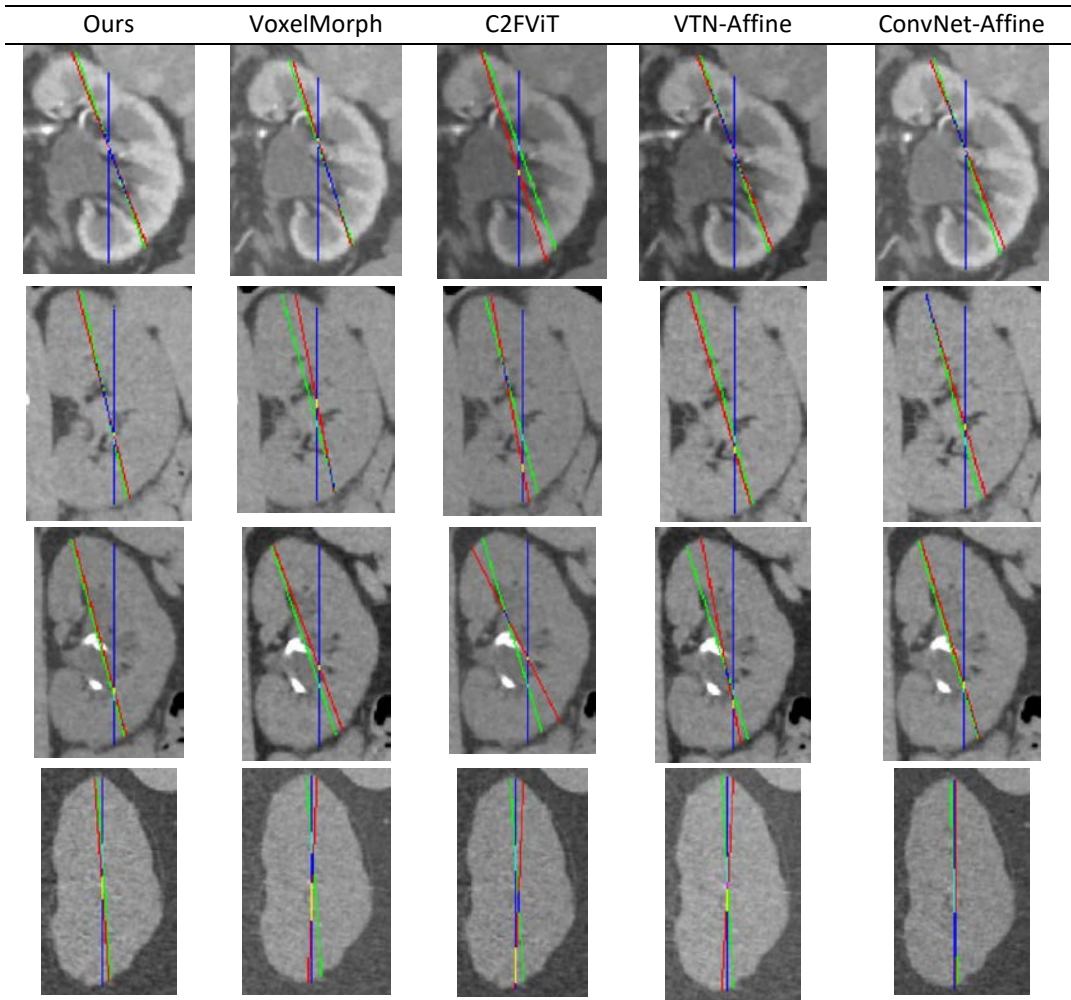


Figure 4. Example of U/S plane in CT volume, displayed in coronal view. blue: initial position, green, reference position, red: registration position.